Published in final edited form as:
J Biomech. 2014 June 27; 47(9): 2035–2042. doi:10.1016/j.jbiomech.2013.10.029.

Murine patellar tendon biomechanical properties and regional strain patterns during natural tendon-to-bone healing after acute injury

Steven D. Gilday[a,b,*], **E. Chris Casstevens**[c], **Keith Kenter**[c], **Jason T. Shearn**[a], and **David L. Butler**[a]

Steven D. Gilday: gildays@mail.uc.edu

[a]Biomedical Engineering Program, University of Cincinnati, Cincinnati, OH, United States

[b]Medical Scientist Training Program, University of Cincinnati, Cincinnati, OH, United States

[c]Department of Orthopaedic Surgery, University of Cincinnati, Cincinnati, OH, United States

Abstract

Tendon-to-bone healing following acute injury is generally poor and often fails to restore normal tendon biomechanical properties. In recent years, the murine patellar tendon (PT) has become an important model system for studying tendon healing and repair due to its genetic tractability and accessible location within the knee. However, the mechanical properties of native murine PT, specifically the regional differences in tissue strains during loading, and the biomechanical outcomes of natural PT-to-bone healing have not been well characterized. Thus, in this study, we analyzed the global biomechanical properties and regional strain patterns of both normal and naturally healing murine PT at three time points (2, 5, and 8 weeks) following acute surgical rupture of the tibial enthesis. Normal murine PT exhibited distinct regional variations in tissue strain, with the insertion region experiencing approximately 2.5 times greater strain than the midsubstance at failure (10.80 ± 2.52% vs. 4.11 ± 1.40%; mean ± SEM). Injured tendons showed reduced structural (ultimate load and linear stiffness) and material (ultimate stress and linear modulus) properties compared to both normal and contralateral sham-operated tendons at all healing time points. Injured tendons also displayed increased local strain in the insertion region compared to contralateral shams at both physiologic and failure load levels. 93.3% of injured tendons failed at the tibial insertion, compared to only 60% and 66.7% of normal and sham tendons, respectively. These results indicate that 8 weeks of natural tendon-to-bone healing does not restore normal biomechanical function to the murine PT following injury.

Keywords

Patellar tendon; Tendon-to-bone healing; Insertion site; Regional strain

*Corresponding author at: Biomedical Engineering Program, 827 Engineering Research Center, 2901 Woodside Drive, Cincinnati, OH 45221, United States. Tel.: +1 513 253 9351; fax: +1 513 556 4162.

Conflict of interest statement: The authors have no conflicts of interest and nothing to disclose.

1. Introduction

Tendon injuries occur in a diverse patient population and commonly result in pain, disability, and significant healthcare costs (United States Bone and Joint Initiative, 2011). Frequently injured tendons include the Achilles, patellar, and quadriceps tendons of the lower extremity, the biceps and rotator cuff tendons of the upper extremity, and the flexor and extensor tendons of the hands (Clayton and Court-Brown, 2008). Treatment of such injuries routinely requires reattachment of a ruptured tendon to its bony insertion, but this presents a challenge due to the extreme difference in material properties between soft and hard tissue. To cope with this material mismatch, the uninjured tendon-to-bone insertion site, also known as the enthesis, exhibits a gradual transition between the compliant tendon and the much stiffer bone via a fibrocartilaginous transition region (Benjamin et al., 2002). Gradations in matrix composition, collagen alignment, cell phenotype, and mineralization (Genin et al., 2009; Thomopoulos et al., 2003; Thomopoulos et al., 2006) help facilitate optimal force transmission while also dissipating potentially damaging interfacial stress concentrations between these mechanically dissimilar materials (Liu et al., 2011; Shaw and Benjamin, 2007). Unfortunately, once disrupted, the insertion site does not regenerate its complex natural architecture and is instead replaced by scar tissue, resulting in a mechanically inferior interface that is susceptible to further injury (Galatz et al., 2006; Kinneberg et al., 2011; Newsham-West et al., 2007; Rodeo et al., 1993).

Functional tissue engineering (FTE), an evolving discipline which emphasizes the restoration of normal mechanical function in damaged load-bearing tissues, has been proposed as a promising alternative to traditional tendon repair strategies (Butler et al., 2000; Guilak et al., 2003). Fundamental to the FTE paradigm is the need to measure the biomechanical properties of normal and naturally healing tissues under physiologic as well as failure loads in order to establish quantitative benchmarks against which tissue-engineered repairs can be compared (Butler et al., 2000). Working towards this goal, our research group determined that in vivo patellar tendon (PT) forces in the rabbit (Juncosa et al., 2003) and goat (Korvick et al., 1996) reached 21% and 40% of normal PT failure force, respectively, during simulated activities of daily living (ADLs). Then, using these physiologic force thresholds as mechanical benchmarks, we evaluated the relative success of various tissue-engineered tendon repairs in a full-length rabbit PT defect model (Butler et al., 2008). Although this FTE approach did yield improved mechanical outcomes compared to natural healing alone, the vast majority of our tissue-engineered PT repairs still fail prematurely at the distal insertion, indicating a need for better strategies to stimulate tendon-to-bone healing.

More recently, our attempts to regenerate functional tendon–bone interfaces have necessitated moving from large animal models such as the rabbit to the more genetically tractable mouse. The availability of transgenic and knockout mice has permitted detailed studies of PT enthesis development (Liu et al., 2012; Liu et al., 2013; Sugimoto et al., 2013) and PT natural healing (Dyment et al., 2012; Dyment et al., 2013; Scott et al., 2011). Lower costs and higher throughputs also make murine models an attractive option for screening the efficacy of novel therapeutic treatments for tendon-to-bone healing before scaling up to more clinically relevant model systems. However, applying the FTE paradigm to PT repair

in the mouse has proven difficult because the peak in vivo forces in the murine PT are unknown and the mechanical properties of native murine PT, specifically the regional (insertion site vs. midsubstance) differences in tissue strains during loading, have not been adequately described. Furthermore, the biomechanical outcomes of natural tendon-to-bone healing after murine PT enthesis injury have not been well characterized.

Thus, the objective of this study was to analyze the global biomechanical properties and regional strain patterns of (1) *normal* murine PT and (2) *naturally healing* murine PT at three time points (2, 5, and 8 weeks) following acute surgical rupture of the tibial enthesis. We hypothesized that normal murine PT would exhibit regional variations in tissue strain, with the more compliant insertion region experiencing larger strain than the stiffer midsubstance. We also hypothesized that at all time points following enthesis injury, healing tendons would exhibit reduced global biomechanical properties and increased strain in the insertion region compared to contralateral shams, resulting in failure initiation at the insertion site.

2. Materials and methods

2.1. Experimental design

Patellar tendon dimensions, structural and material properties, regional strain patterns, and failure locations were assessed at three different post-injury time points (2, 5, and 8 weeks) in a cohort of 30 twenty-week-old (20.3 ± 0.5 weeks; mean ± SD) male CD-1 wild-type mice. Twenty-week-old mice were chosen for this study because they are skeletally mature adults whose patellar tendons are large enough to allow for the creation of standardized, repeatable surgical injuries and the biomechanical testing of normal and healing tissues in vitro. The study time points were carefully selected in order to capture both the proliferative and remodeling phases of tendon healing and to keep consistent with our group's previous work on natural healing of murine PT (Dyment et al., 2012). Following surgical injury, naturally healing tendons (n=10 per time point) were directly compared with contralateral shams (n=10 per time point). Inter-animal comparisons were also made using a separate group of normal, unoperated patellar tendons (n=10) from healthy twenty-week-old male CD-1 mice.

2.2. Murine patellar tendon injury model

All murine surgeries were performed by one coauthor (ECC) and were approved by the University of Cincinnati Institutional Animal Care and Use Committee. Mice were anesthetized with 4% isofluorane, subcutaneously injected with 1 mg/kg buprenorphine, and both hind limbs were shaved and aseptically prepped. Using surgical loupes (2.5 ×), small (0.5–1 cm) longitudinal skin incisions were made to expose the PT in each limb. An acute surgical injury was then created in the left PT while the contralateral PT was subjected to a sham procedure.

2.2.1. Surgical injury (Fig. 1A)—Using a previously described surgical technique (Dyment et al., 2012), two full-length longitudinal incisions were created in the left PT in order to isolate the central-third portion of the tendon from adjacent medial and lateral struts.

The central-third of the PT was then transected at its distal insertion into the tibia. Any remaining soft tissue at the insertion site was removed with microsurgical scissors and the enthesis was further disrupted by using a small jigsaw blade to create a shallow bony defect. Care was taken not to damage the intact struts. The tendon's proximal patellar insertion was also left intact. The transected central-third was laid back in its normal anatomic position between the struts with the distal end in close proximity to its original insertion site on the tibia, but no attempt was made to physically reattach the tendon tissue to the bone.

2.2.2. Contralateral sham (Fig. 1B)—The central-third of the right PT was isolated from the struts as described above but was not transected at the distal insertion. Thus, sham-operated tendons retained a structurally intact tendon–bone interface at both the tibial and patellar ends.

In both injured and sham limbs, skin incisions were closed with 5–0 prolene suture. Mice were allowed full range of motion and unlimited cage activity immediately following surgery. No gait alterations or behavioral changes were noted as a result of the surgical procedure. At the designated post-surgical time point (2, 5, or 8 weeks), mice were euthanized by carbon dioxide asphyxiation and frozen at −20 °C to await biomechanical testing.

2.3. Biomechanical testing and analysis

On the day of testing, murine hind limbs were thawed and dissected to expose the PT. After noting gross morphological appearance, the central-third of each PT was isolated by dissecting away the medial and lateral struts. Using 6–0 silk suture soaked in Verhoeff's stain, tendons were marked with three horizontal stain lines located just distal to the tibial insertion, approximately 1 mm proximal to the tibial insertion, and approximately 2 mm proximal to the tibial insertion, respectively. The stain lines clearly delineated the insertion region (defined in this study as the distal 1/3 of the PT) from the midsubstance region (the central 1/3 of the PT). Tibia– central-third PT–patella units were mounted in a materials testing system (100R, Test Resources) by embedding the tibia in the upper grip with polymethylmethacrylate and fixing it in place with a metal staple, then securing the patella in a preexisting, conical-shaped lower grip (Fig. 2A). Once mounted, tendons were submerged in PBS at 37 °C and preloaded to 0.02 N (Dyment et al., 2012). High resolution (∼6 um/pixel) digital images were taken in both the frontal and sagittal planes in order to calculate initial tendon dimensions. Following a preconditioning phase (25 cycles, 0–1% strain, 0.003 mm/s), specimens were failed in uniaxial tension at a rate of 0.003 mm/s while recording grip-to-grip displacement and load (Dyment et al., 2012). Images of the tendon's anterior surface were captured at 15 s intervals throughout the failure test in order to optically measure regional tissue strains and assess failure location.

Ultimate load, displacement at failure, ultimate stress, and strain at failure were recorded for each PT specimen. Using an automated linear regression algorithm, stiffness and modulus were calculated from the linear region of the load– displacement and stress–strain curves, respectively. Regional tissue strains were calculated by optically tracking the applied stain lines. For each specimen, the digital images captured during the failure test were stacked,

cropped, and thresholded so that frame-by-frame centroid displacements of the stain lines could be automatically tracked using the MTrack2 plugin for ImageJ (Fig. 2B–D). This raw displacement data was used to calculate and plot the tensile strain in both the distal insertion and midsubstance regions as a function of load. Failure location (tibial insertion, midsubstance, or patellar grip) was also noted for each specimen.

2.4. Statistical analysis

All data were verified to be normal and homoscedastic prior to statistical testing. Two-way factorial ANOVA was used to determine the main effects of surgical treatment and time post-surgery on PT cross-sectional area, structural properties, material properties, and regional tissue strains. At each time point (2, 5, and 8 weeks), significance between treatment groups (normal, sham, injury) was assessed using one-way ANOVA followed by Fisher's least significant difference (LSD) post-hoc comparisons. The effect of treatment on failure location was evaluated using multinomial logistic regression. Significance was set at $p < 0.05$. All statistical testing was performed using IBM SPSS Statistics 21.0.

3. Results

3.1. Gross morphology and tendon dimensions

At 2 weeks post-injury, gross observation revealed dark pink granulation tissue at the healing tendon–bone interface and a thickened, fibrotic paratenon on both the anterior and posterior surfaces of the PT. At 5 and 8 weeks post-injury, the scar-like repair tissue at the insertion site appeared more integrated with the underlying bone and adjacent struts but remained discolored. Fibrous adhesions to subcutaneous connective tissue or the infrapatellar fat pad were present in some specimens. At all post-surgical time points, the injured tendons exhibited significantly increased cross-sectional area compared to both normal and contralateral sham tendons ($p < 0.05$; Table 1). The sham procedure resulted in mild fibrosis on the surface of the PT but did not significantly affect tendon cross-sectional area.

3.2. Structural and material properties

Surgical treatment and time post-surgery each significantly affected PT structural and material properties. Injured tendons displayed significantly reduced ultimate load, linear stiffness, ultimate stress, and linear modulus at both 2 and 5 weeks post-surgery compared to normal and sham tendons ($p < 0.05$; Table 1, Figs. 3A and 4). Although ultimate load had returned to 87% of normal values by 8 weeks post-surgery ($p=0.139$), linear stiffness, ultimate stress, and linear modulus only reached 79%, 49%, and 42% of normal values, respectively ($p < 0.05$; Fig. 4). The ultimate load and ultimate stress of the injured tendons increased linearly over time, whereas linear stiffness and linear modulus increased significantly only between 2 and 5 weeks post-surgery ($p < 0.001$ in both cases), plateauing between the 5 and 8 week time points ($p=0.817$ and $p=0.784$, respectively; Fig. 4). None of the structural or material properties of the sham-operated tendons were significantly different from normal at any of the post-surgical time points (Table 1, Figs. 3B and 4).

3.3. Regional tissue strains

Normal, unoperated murine PTs exhibited distinct regional variations in tissue strain (Fig. 5). At all load levels greater than 0.5 N, average local strains in the insertion region were 2–3 times greater than corresponding strains in the tendon midsubstance. In both the insertion and midsubstance regions, a non-linear relationship appeared to exist between load and strain. As load increased from 0 to 1 N, strain in the insertion and midsubstance regions increased rapidly, but as load continued to increase past 1 N, the resulting increases in local strain became less pronounced. At failure, insertion strain had reached a maximum value of 10.80 ± 2.52% (mean ± SEM) whereas midsubstance strain had plateaued at a maximum value of only 4.11 ± 1.40%.

Tendons subjected to an enthesis injury showed increased local strain in the insertion region compared to normal tendons at all time points (Fig. 6A). As expected, the healing tissue at the insertion site was more compliant than the normal enthesis, with strain at failure reaching a maximum of 18.85 ± 4.37% after 8 weeks of healing. The sham procedure did not affect local strain in the insertion region (Fig. 6C). Surprisingly, both the injury and sham treatments produced an increase in midsubstance strain compared to normal tendons (Fig. 6B and D). Factors such as inflammation, disruption of normal blood supply, altered mechanical loading, or tissue fibrosis in response to the surgical procedure may have contributed to the increased local strain in the midsubstance.

Since the small size of the mouse prevents direct in vivo measurement of PT forces, we chose to assess local strains in the insertion and midsubstance at 21% and 40% of normal PT failure force, which correspond to the peak in vivo forces measured in the rabbit (Juncosa et al., 2003) and goat (Korvick et al., 1996) patellar tendon, respectively. At these physiologic load levels, local strains in the insertion region were significantly increased in injured tendons compared to contralateral shams at the 5 and 8 week time points ($p < 0.05$; Fig. 7), indicating that the natural healing process was unable to regenerate a mechanically normal enthesis over this time period. Local strains in the tendon midsubstance did not differ between the injured and sham groups (Fig. 7).

3.4. Failure location

Surgical treatment was found to be a significant predictor of failure location (p=0.043). Twenty-eight out of 30 injured tendons (93.3%) failed at the tibial insertion compared to only 60% and 66.7% of normal and sham tendons, respectively (Fig. 8A). Although the insertion was the most common site of failure in all treatment groups, tendons subjected to a surgical injury were 1.4 times as likely to fail at the insertion site compared to sham tendons (p=0.041). Normal and sham tendons often failed via a delamination mechanism in which the anterior and posterior portions of the tendon separated and slid past one another (Fig. 8B). In contrast, surgically injured tendons most often failed via a transverse rupture of the repair tissue at the tendon–bone junction (Fig. 8C).

4. Discussion

The objective of this study was to analyze the global biomechanical properties and regional strain patterns of both normal and naturally healing murine PT at 2, 5, and 8 weeks

following acute surgical rupture of the tibial enthesis. Our first hypothesis was that normal murine PT would exhibit regional variations in tissue strain, with the more compliant insertion region experiencing larger strain than the stiffer midsubstance. By optically tracking surface strain markers during biomechanical testing, we found that local strains in the insertion region were 2–3 times greater than corresponding strains in the midsubstance at all load levels greater than 0.5 N. At failure, the insertion region had experienced 10.80 ± 2.52% strain (mean ± SEM) compared to only 4.11 ± 1.40% in the midsubstance. In addition to our findings in the murine PT, regional variations in local tissue strain have been recorded in human patellar (Butler et al., 1990; Haraldsson et al., 2005) and supraspinatus (Huang et al., 2005) tendon specimens, as well as in rat tibialis anterior (Arruda et al., 2006; Wu et al., 2004), murine Achilles (Rigozzi et al., 2009), and frog semitendonosis (Lieber et al., 1991) tendons. These results imply that normal tendon biomechanical properties vary along the tendon length, likely due to differences in tissue composition and structure between the midsubstance and insertion regions (Thomopoulos et al., 2003) or as a result of adaptation to subtle differences in the in vivo loading environment (Benjamin and Ralphs, 1998; Doschak and Zernicke, 2005; Malliaras et al., 2013). In fact, differences in collagen crimp pattern at rest and fiber realignment during mechanical loading exist between the tendon insertion and midsubstance (Lake et al., 2010; Miller et al., 2012; Stouffer et al., 1985), which may explain the observed differences in strain pattern.

Our second hypothesis was that at all time points following enthesis injury, healing tendons would exhibit reduced global biomechanical properties and increased strain in the insertion region compared to contralateral shams, resulting in failure initiation at the insertion site. Although ultimate loads returned to 87% of normal levels in the injured tendons at 8 weeks post-surgery, linear stiffness, ultimate stress, and linear modulus remained significantly inferior to normal and shams at all time points. Injured tendons also displayed increased local strain in the insertion region at both physiologic and failure load levels. Additionally, 93.3% of injured tendons failed at the tibial insertion, compared to only 60% and 66.7% of normal and sham tendons, respectively. Taken as a whole, these results indicate that 8 weeks of natural tendon-to-bone healing does not restore normal biomechanical function to the murine PT following an acute injury to the tibial enthesis. Studies of tendon-to-bone healing in other injury models have reported similar results. For example, the rat supraspinatus tendon also exhibits impaired biomechanical properties after 8 weeks of tendon-to-bone healing following acute injury (Galatz et al., 2006). Interestingly, biomechanical outcomes in our injury model (in which the central-third of the PT was transected at the tibial insertion and the damaged flap of tendon tissue left in place to heal back to the bone) were no better than in a full-length, full-thickness central-third murine PT defect model (in which the central-third of the tendon was completely removed, leaving an empty defect; Dyment et al., 2012). This finding, coupled with the fact that cross-sectional area increased significantly in the injured tendons, indicates that failed healing is not the result of a lack of new tissue formation, but instead is due to the inability of the healing soft tissue to reintegrate with bone.

There were limitations to our study. (1) After creating the acute injury, we did not attempt to repair or reattach the injured tendon to the underlying bone. Thus, this particular model is not representative of a surgical tendon repair, but instead mimics unaided tendon-to-bone

healing in a load-protected environment in which the healing central-third PT is under no initial tension. (2) Only the central-third portion of the PT was biomechanically tested, and so any changes in the struts in response to the injury or sham procedure would not have been detected. This is an important consideration, since the intrinsic tendon healing response may actually initiate in the paratenon surrounding the defect (Dyment et al., 2013), and any adaptations due to altered loading in the struts following injury could contribute significantly to overall tendon biomechanics. (3) In this study, we calculated global tissue strain based on grip-to-grip displacement measurements, but we calculated local tissue strain by optically tracking stain lines on the anterior surface of the PT during the failure test. It is well known that these two techniques for estimating strain do not always produce equivalent results (Butler et al., 1984; Wu et al., 2004), and in our study, normal murine PT experienced grip-to-grip strains in excess of 20% at failure but local strain measurements in the insertion and midsubstance regions never exceeded 12%. However, we did not measure local strains in the most proximal region of the PT, and large strains in this tissue region could have accounted for the apparent discrepancy.

The results of this study indicate that 8 weeks of natural tendon-to-bone healing does not restore normal biomechanical function to the acutely injured murine PT enthesis. Although we focused only on biomechanical outcomes, biological repair outcomes also need to be assessed in future studies in order to better understand the linkages between tendon biology and mechanics. Evaluating cell phenotype, gene expression, matrix composition, and collagen alignment in the healing tissue would help reveal the underlying biological differences compared to the normal enthesis, which in turn could help explain the observed alterations in mechanics. Moving forward, this murine PT injury model will be used to test the efficacy of novel biologic treatments for tendon-to-bone healing, including new functional tissue engineering strategies aimed at regenerating a normal tendon–bone interface.

Acknowledgments

We gratefully acknowledge the National Institutes of Health for providing research support (R01 AR056943) as well as student funding via the University of Cincinnati MSTP training grant (T32 GM063483). We also thank Andrew Breidenbach, Cindi Gooch, and Andrea Lalley for their assistance during animal surgeries and Dr. Lou Soslowsky for his valuable contributions to our current biomechanical testing protocols.

References

Arruda EM, Calve S, Dennis RG, Mundy K, Baar K. Regional variation of tibialis anterior tendon mechanics is lost following denervation. J Appl Physiol (Bethesda, Md: 1985). 2006; 101:1113–1117.

Benjamin M, Kumai T, Milz S, Boszczyk BM, Boszczyk AA, Ralphs JR. The skeletal attachment of tendons—tendon “entheses”. Comp Biochem Physiol Part A, Mol Integr Physiol. 2002; 133:931–945.

Benjamin M, Ralphs JR. Fibrocartilage in tendons and ligaments–an adaptation to compressive load. J Anat. 1998; 193(Pt 4):481–494. [PubMed: 10029181]

Butler DL, Goldstein SA, Guilak F. Functional tissue engineering: the role of biomechanics. J Biomech Eng. 2000; 122:570–575. [PubMed: 11192376]

Butler DL, Grood ES, Noyes FR, Zernicke RF, Brackett K. Effects of structure and strain measurement technique on the material properties of young human tendons and fascia. J Biomech. 1984; 17:579–596. [PubMed: 6490671]

Butler DL, Juncosa-Melvin N, Boivin GP, Galloway MT, Shearn JT, Gooch C, Awad H. Functional tissue engineering for tendon repair: a multi-disciplinary strategy using mesenchymal stem cells, bioscaffolds, and mechanical stimulation. J Orthop Res: Off Publ Orthop Res Soc. 2008; 26:1–9.

Butler DL, Sheh MY, Stouffer DC, Samaranayake VA, Levy MS. Surface strain variation in human patellar tendon and knee cruciate ligaments. J Biomech Eng. 1990; 112:38–45. [PubMed: 2308302]

Clayton RA, Court-Brown CM. The epidemiology of musculoskeletal tendinous and ligamentous injuries. Injury. 2008; 39:1338–1344. [PubMed: 19036362]

Doschak MR, Zernicke RF. Structure, function and adaptation of bone–tendon and bone–ligament complexes. J Musculoskelet Neuronal Interact. 2005; 5:35–40. [PubMed: 15788869]

Dyment NA, Kazemi N, Aschbacher-Smith LE, Barthelery NJ, Kenter K, Gooch C, Shearn JT, Wylie C, Butler DL. The relationships among spatiotemporal collagen gene expression, histology, and biomechanics following full-length injury in the murine patellar tendon. J Orthop Res: Off Publ Orthop Res Soc. 2012; 30:28–36.

Dyment NA, Liu CF, Kazemi N, Aschbacher-Smith LE, Kenter K, Breidenbach AP, Shearn JT, Wylie C, Rowe DW, Butler DL. The paratenon contributes to scleraxis-expressing cells during patellar tendon healing. PLoS One. 2013; 8:e59944. [PubMed: 23555841]

Galatz LM, Sandell LJ, Rothermich SY, Das R, Mastny A, Havlioglu N, Silva MJ, Thomopoulos S. Characteristics of the rat supraspinatus tendon during tendon-to-bone healing after acute injury. J Orthop Res: Off Publ Orthop Res Soc. 2006; 24:541–550.

Genin GM, Kent A, Birman V, Wopenka B, Pasteris JD, Marquez PJ, Thomopoulos S. Functional grading of mineral and collagen in the attachment of tendon to bone. Biophys J. 2009; 97:976–985. [PubMed: 19686644]

Guilak, F.; Butler, DL.; Goldstein, SA.; Mooney, D. Functional Tissue Engineering. Springer; New York: 2003. p. 426

Haraldsson BT, Aagaard P, Krogsgaard M, Alkjaer T, Kjaer M, Magnusson SP. Region-specific mechanical properties of the human patella tendon. J Appl Physiol (Bethesda, Md: 1985). 2005; 98:1006–1012.

Huang CY, Wang VM, Pawluk RJ, Bucchieri JS, Levine WN, Bigliani LU, Mow VC, Flatow EL. Inhomogeneous mechanical behavior of the human supraspinatus tendon under uniaxial loading. J Orthop Res: Off Publ Orthop Res Soc. 2005; 23:924–930.

Juncosa N, West JR, Galloway MT, Boivin GP, Butler DL. In vivo forces used to develop design parameters for tissue engineered implants for rabbit patellar tendon repair. J Biomech. 2003; 36:483–488. [PubMed: 12600338]

Kinneberg KR, Galloway MT, Butler DL, Shearn JT. Effect of implanting a soft tissue autograft in a central-third patellar tendon defect: biomechanical and histological comparisons. J Biomech Eng. 2011; 133:091002. [PubMed: 22010737]

Korvick DL, Cummings JF, Grood ES, Holden JP, Feder SM, Butler DL. The use of an implantable force transducer to measure patellar tendon forces in goats. J Biomech. 1996; 29:557–561. [PubMed: 8964786]

Lake SP, Miller KS, Elliott DM, Soslowsky LJ. Tensile properties and fiber alignment of human supraspinatus tendon in the transverse direction demonstrate inhomogeneity, nonlinearity, and regional isotropy. J Biomech. 2010; 43:727–732. [PubMed: 19900677]

Lieber RL, Leonard ME, Brown CG, Trestik CL. Frog semitendinosis tendon load–strain and stress–strain properties during passive loading. Am J Physiol. 1991; 261:C86–C92. [PubMed: 1858862]

Liu CF, Aschbacher-Smith L, Barthelery NJ, Dyment N, Butler D, Wylie C. Spatial and temporal expression of molecular markers and cell signals during normal development of the mouse patellar tendon. Tissue Eng Part A. 2012; 18:598–608. [PubMed: 21939397]

Liu CF, Breidenbach A, Aschbacher-Smith L, Butler D, Wylie C. A role for hedgehog signaling in the differentiation of the insertion site of the patellar tendon in the mouse. PLoS One. 2013; 8:e65411. [PubMed: 23762363]

Liu Y, Birman V, Chen C, Thomopoulos S, Genin GM. Mechanisms of bimaterial attachment at the interface of tendon to bone. J Eng Mater Technol. 2011; 133:011006. [PubMed: 21743758]

Malliaras P, Kamal B, Nowell A, Farley T, Dhamu H, Simpson V, Morrissey D, Langberg H, Maffulli N, Reeves ND. Patellar tendon adaptation in relation to load-intensity and contraction type. J Biomech. 2013; 46:1893–1899. [PubMed: 23773532]

Miller KS, Connizzo BK, Feeney E, Soslowsky LJ. Characterizing local collagen fiber re-alignment and crimp behavior throughout mechanical testing in a mature mouse supraspinatus tendon model. J Biomech. 2012; 45:2061–2065. [PubMed: 22776688]

Newsham-West R, Nicholson H, Walton M, Milburn P. Long-term morphology of a healing bone–tendon interface: a histological observation in the sheep model. J Anat. 2007; 210:318–327. [PubMed: 17331180]

Rigozzi S, Muller R, Snedeker JG. Local strain measurement reveals a varied regional dependence of tensile tendon mechanics on glycosaminoglycan content. J Biomech. 2009; 42:1547–1552. [PubMed: 19394024]

Rodeo SA, Arnoczky SP, Torzilli PA, Hidaka C, Warren RF. Tendon-healing in a bone tunnel. A biomechanical and histological study in the dog. J Bone Jt Surg Am. 1993; 75:1795–1803.

Scott A, Sampaio A, Abraham T, Duronio C, Underhill TM. Scleraxis expression is coordinately regulated in a murine model of patellar tendon injury. J Orthop Res: Off Publ Orthop Res Soc. 2011; 29:289–296.

Shaw HM, Benjamin M. Structure-function relationships of entheses in relation to mechanical load and exercise. Scand J Med Sci Sports. 2007; 17:303–315. [PubMed: 17490450]

Stouffer DC, Butler DL, Hosny D. The relationship between crimp pattern and mechanical response of human patellar tendon–bone units. J Biomech Eng. 1985; 107:158–165. [PubMed: 3999712]

Sugimoto Y, Takimoto A, Akiyama H, Kist R, Scherer G, Nakamura T, Hiraki Y, Shukunami C. Scx^{+}/$Sox9^{+}$ progenitors contribute to the establishment of the junction between cartilage and tendon/ligament. Development (Cambridge, England). 2013; 140:2280–2288.

Thomopoulos S, Marquez JP, Weinberger B, Birman V, Genin GM. Collagen fiber orientation at the tendon to bone insertion and its influence on stress concentrations. J Biomech. 2006; 39:1842–1851. [PubMed: 16024026]

Thomopoulos S, Williams GR, Gimbel JA, Favata M, Soslowsky LJ. Variation of biomechanical, structural, and compositional properties along the tendon to bone insertion site. J Orthop Res: Off Publ Orthop Res Soc. 2003; 21:413–419.

United States Bone and Joint Initiative. The Burden of Musculoskeletal Diseases in the United States. Second. American Academy of Orthopaedic Surgeons; Rosemont, IL: 2011.

Wu JZ, Brumfield A, Miller GR, Metheny R, Cutlip RG. Comparison of mechanical properties of rat tibialis anterior tendon evaluated using two different approaches. Biomed Mater Eng. 2004; 14:13–22. [PubMed: 14757949]

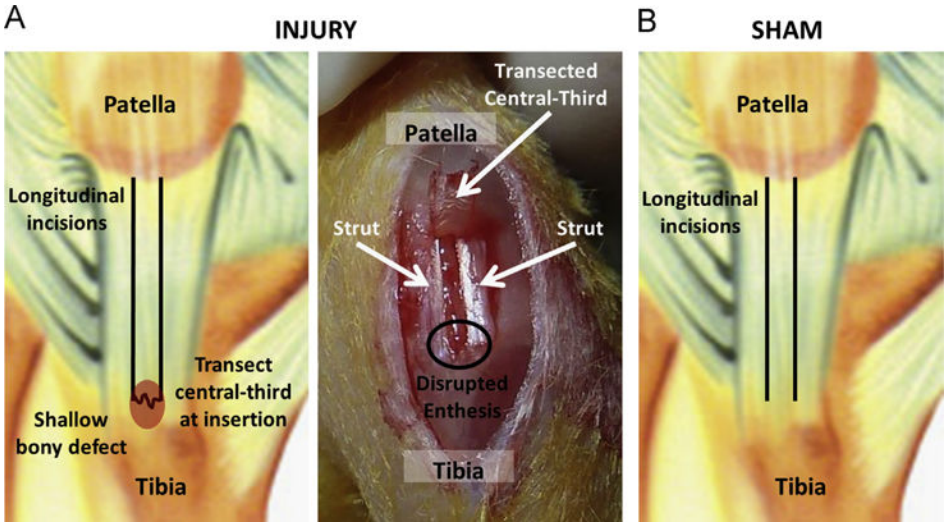

Fig. 1.

Murine patellar tendons were subjected to either an acute surgical injury or a contralateral sham procedure. To create the surgical injury (A), two full-length longitudinal incisions were made to isolate the central third of the tendon, which was then transected at the tibial insertion. A shallow bony defect was created in the tibia and the transected central-third was laid back in its normal anatomic position between the medial and lateral struts to facilitate tendon-to-bone healing. For the contralateral sham procedure (B), longitudinal incisions were made to isolate the central third of the tendon, but the tibial insertion was left intact.

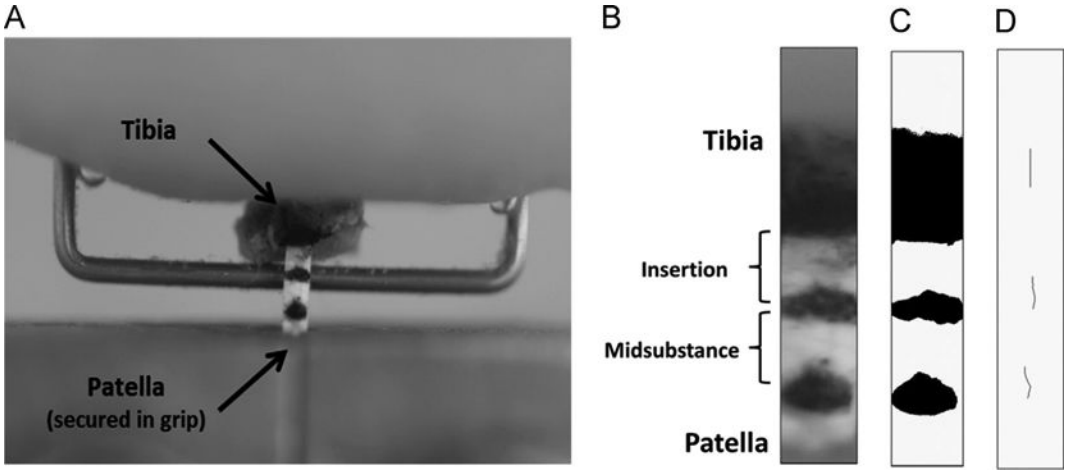

Fig. 2.

Central-third patellar tendon specimens were marked with three stain lines and loaded into a tensile testing system by embedding the tibia in polymethylmethacrylate, fixing the bone in place with a metal staple, then securing the patella in a conical-shaped grip (A). To calculate local tissue strain in the insertion and midsubstance regions, high resolution images were captured at 15 s intervals during the failure test (B) and thresholded (C) so that the frame-by-frame displacement of each optical strain marker could be tracked using the MTrack2 plugin for ImageJ (D).

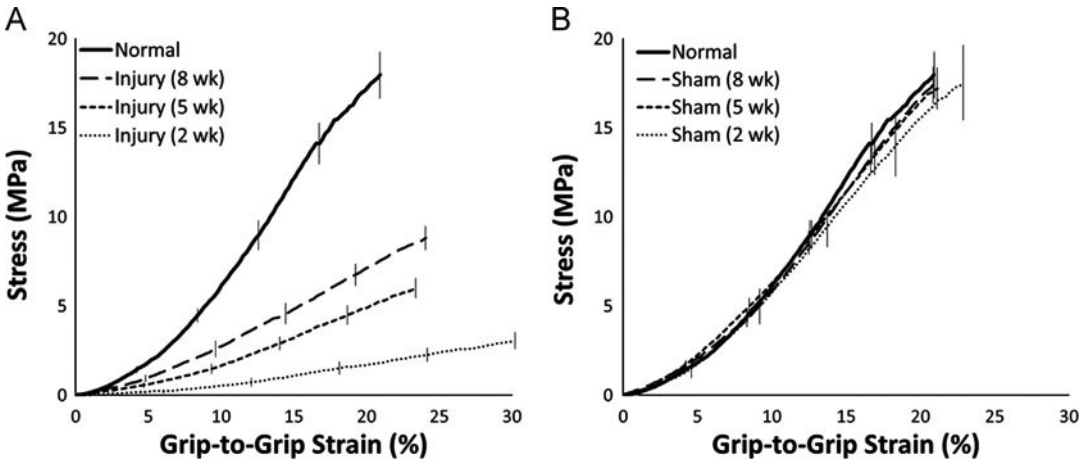

Fig. 3.

Average stress–strain curves for injured and sham tendons at 2, 5, and 8 weeks post-surgery. (A) Injured tendons showed significantly decreased material properties at all time points compared to normal PT ($p < 0.05$). (B) The sham procedure had no effect on material properties at any time point. Error bars indicate SEM; n=10 per group.

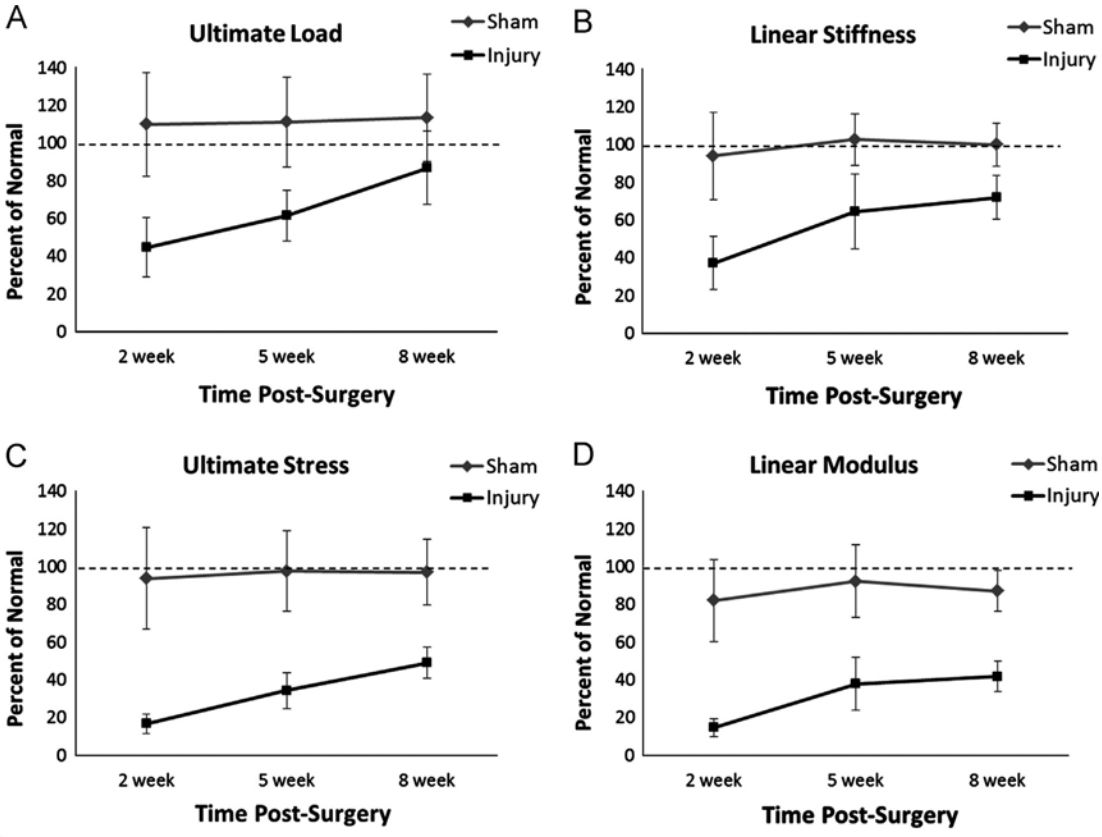

Fig. 4.

Structural and material properties of injured and sham tendons plotted as a percent of normal. With the exception of ultimate load at 8 weeks, injured tendons showed significantly reduced ultimate load (A), linear stiffness (B), ultimate stress (C), and linear modulus (D) compared to both normal and sham at all time points ($p < 0.05$). The ultimate load and ultimate stress of injured tendons increased linearly over time (A and C), whereas linear stiffness and linear modulus increased significantly between 2 and 5 weeks but then plateaued between 5 and 8 weeks (B and D). The sham procedure had no effect on structural or material properties at any time point. Error bars indicate SD; n=10 per group.

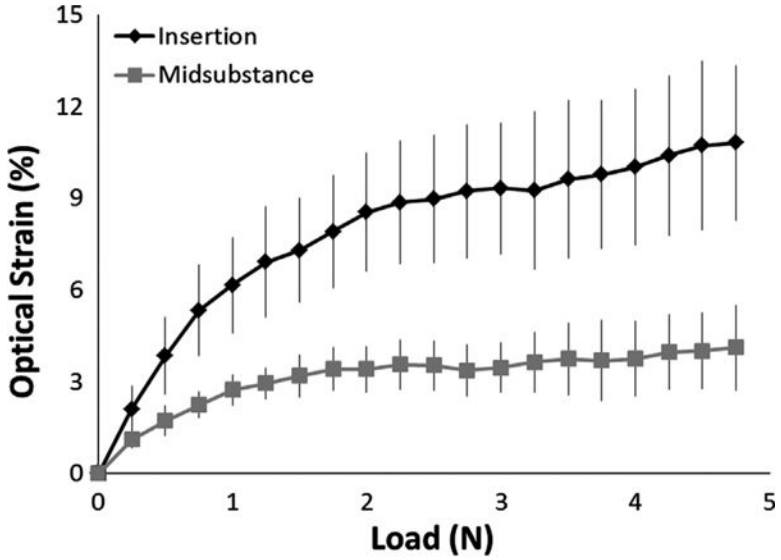

Fig. 5.

Normal murine patellar tendons exhibited distinct regional variations in tissue strain. At all load levels greater than 0.5 N, local strains in the insertion region (top curve) were 2–3 times greater than corresponding strains in the tendon midsubstance (bottom curve). At failure, insertion strain reached a maximum value of 10.80 ± 2.52% (mean ± SEM) compared to only 4.11 ± 1.40% in the midsubstance. The curves represent the average of 10 specimens; error bars indicate SEM.

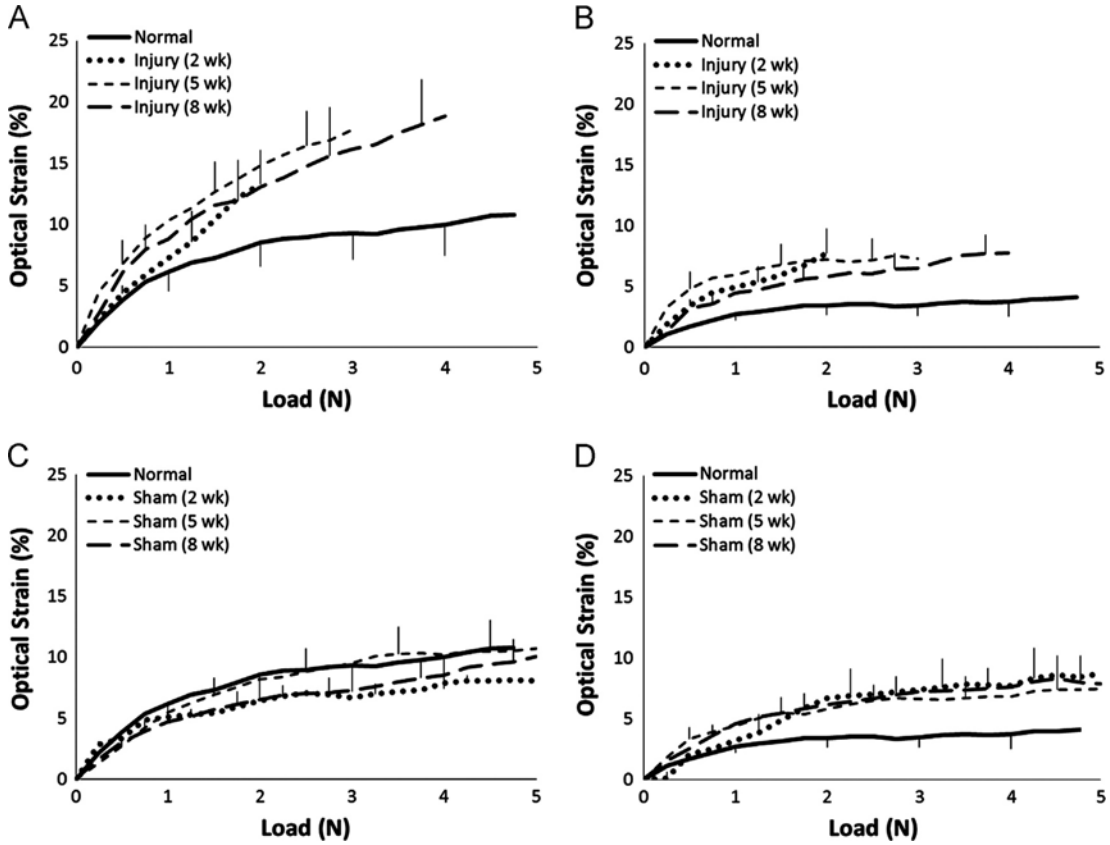

Fig. 6.

Regional strains in injured and sham tendons compared to normal. At all post-surgical time points, insertion strains were increased in injured tendons (A) but not in contralateral shams (C). In contrast, midsubstance strains were increased in both the injured (B) and sham (D) tendons following surgery. Error bars indicate SEM; *n*=10 per group.

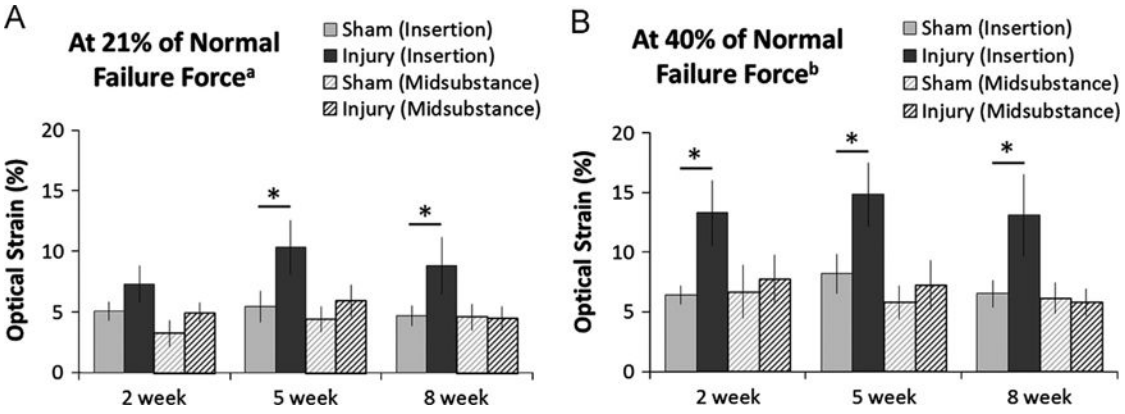

Fig. 7.

Regional strains differed significantly between injured and sham tendons at physiologic load levels. (A) At 21% of normal PT failure force, injured tendons showed increased local strain in the insertion region (solid black bars) compared to contralateral shams (solid gray bars) at both the 5 and 8 week time points (*$p < 0.05$). (B) At 40% of normal PT failure force, injured tendons showed increased local strain in the insertion region (solid black bars) compared to contralateral shams (solid gray bars) at all time points (*$p < 0.05$). No significant differences in midsubstance strain were detected between the injured (hashed black bars) and sham (hashed gray bars) groups at any time point. [a]Peak in vivo forces measured in the rabbit patellar tendon (Juncosa et al., 2003). [b]Peak in vivo forces measured in the goat patellar tendon (Korvick et al., 1996). Error bars indicate SEM; n=10 per group.

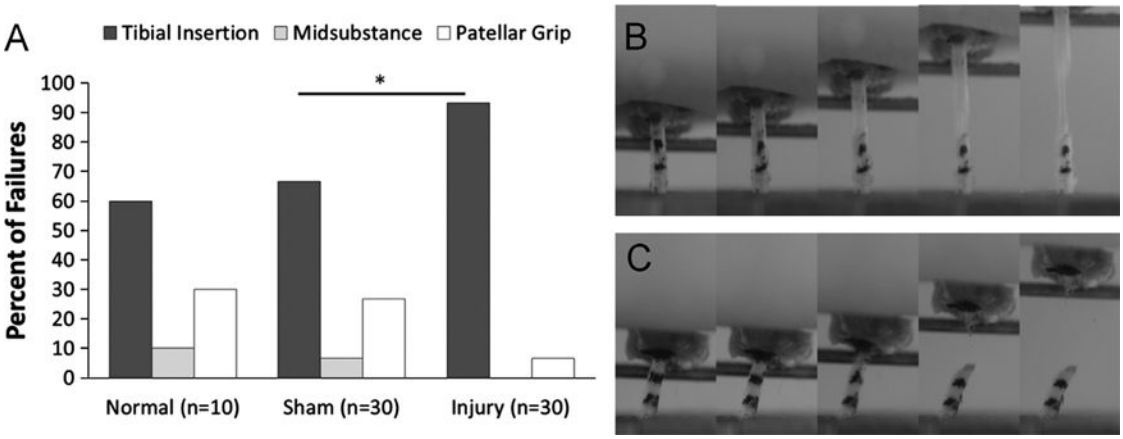

Fig. 8.

Failure location and failure mechanism differed between injured and sham tendons. (A) A higher percentage of injured tendons failed at the tibial insertion compared to contralateral shams (93.3% vs. 66.7%; **p*=0.041). (B) Normal and sham tendons often failed via a delamination mechanism in which the anterior and posterior portions of the tendon separated and slid past one another. (C) Surgically injured tendons most often failed via a transverse rupture of the repair tissue at the tendon–bone junction.

Table 1

Structural and material properties of normal, sham, and injured central-third murine patellar tendons at 2, 5, and 8 weeks post-surgery (n=10 per group; mean ± standard deviation).

	Cross-sectional area (mm^2)	Ultimate load (N)	Stiffness (N/mm)	Ultimate stress (MPa)	Modulus (MPa)
Normal PT	0.26 ± 0.05	4.73 ± 1.03	11.55 ± 2.32	17.96 ± 3.09	140.04 ± 19.60
Sham (2 week)	0.32 ± 0.07	5.19 ± 1.30	10.84 ± 2.68	16.84 ± 4.85	115.04 ± 30.29
Injury (2 week)	0.59 ± 0.09[a,b]	2.11 ± 0.74[a,b]	4.28 ± 1.63[a,b]	3.02 ± 0.93[a,b]	20.49 ± 6.53[a,b]
Sham (5 week)	0.30 ± 0.05	5.25 ± 1.13	11.86 ± 1.58	17.54 ± 3.81	129.37 ± 26.88
Injury (5 week)	0.49 ± 0.10[a,b]	2.90 ± 0.64[a,b]	7.43 ± 2.28[a,b]	6.15 ± 1.71[a,b]	53.05 ± 19.81[a,b]
Sham (8 week)	0.31 ± 0.04	5.36 ± 1.09	11.53 ± 1.32	17.45 ± 3.13	121.95 ± 14.97
Injury (8 week)	0.47 ± 0.07[a,b]	4.10 ± 0.92[b]	8.29 ± 1.34[a,b]	8.82 ± 1.51[a,b]	58.60 ± 11.43[a,b]

[a] Significantly different compared to normal PT.

[b] Significantly different compared to contralateral sham at the same time point.